Non-peer-reviewed preprint submitted to EarthArXiv

The Bhote Koshi–Trishuli flash flood of 26 August 2026, Rasuwa, Nepal: warning latency exceeded flood travel time

Sunim Acharya[1] and Animesh Paudel[2]
[1]Independent researcher, San Francisco, California, United States
[2]Independent researcher, Perth, Western Australia, Australia
Correspondence: sunim.54@gmail.com
ORCID: Acharya 0009-0003-1207-3610, Paudel 0009-0005-3833-2718

Status. This is a non-peer-reviewed preprint posted to EarthArXiv at https://doi.org/10.31223/X5HN5H. This manuscript has not been submitted to a journal for peer review at the time of posting. Any subsequent submission, and the resulting journal DOI, will be recorded in a revised version of this preprint.

Data and code. The validated data package and the analysis that produces every figure and table in this paper are archived at https://doi.org/10.5281/zenodo.22679444, release 3.0.0, under CC-BY-4.0. The concept DOI https://doi.org/10.5281/zenodo.22153581 always resolves to the newest release.

Note on provisional figures. Casualty totals for this event were still being revised by the responsible agencies when this version was prepared. The figures used are dated in the text and in the archived data package, and the analysis depends on the spatial distribution of recoveries rather than on the totals.

The Bhote Koshi–Trishuli flash flood of 26 August 2026, Rasuwa, Nepal: warning latency exceeded flood travel time

Sunim Acharya[1] and Animesh Paudel[2]

[1]Independent researcher, San Francisco, California, United States
[2]Independent researcher, Perth, Western Australia, Australia

Correspondence: Sunim Acharya (sunim.54@gmail.com)

Abstract. An ice–rock mass detached from the northern flank of the Langtang massif, Nepal, at 08:37:10 Nepal Time on 26 August 2026. It blocked the Lhende Khola and released a cascade along the Bhote Koshi–Trishuli–Narayani corridor that killed at least 1357 people and left 5326 missing. This study measures the warning chain end to end, timing the front at six stations from ten-minute stage series recovered from the river-watch service of Nepal's Flood Forecasting Division. The mass public alert followed the trigger by 38.8 min while the wave reached the uppermost gauge within 12.8 min, giving lead times of -26 to -16 min at the first inhabited settlement and $+4$ to $+14$ min at the next. Three destroyed gauges were lost at 27, 69 and 87 % of their warning stages, so threshold logic never fired. Fatalities concentrated where lead time was negative or negligible, while districts warned hours in advance received most of the bodies. A closed-form energy budget rules out frictional meltwater as the source. Supplying the measured 19.96×10^6 m^3 excess volume would require melting four times the ice in the 2021 Chamoli detachment. Lead time rather than flood magnitude set the limit on survival.

1 Introduction

High-mountain Asia supplies water to roughly a quarter of the world's population from a cryosphere in rapid retreat (Immerzeel et al., 2020), and it is producing large ice–rock detachments faster than warning systems are being adapted. The 2016 Aru twin collapses (Kääb et al., 2018), the 2021 Chamoli disaster (Shugar et al., 2021) and recurrent Sedongpu failures on the Yarlung Tsangpo (Li et al., 2022) established that glacierised bedrock slopes can fail at 10^7–10^8 m^3 with little warning, and more often than was assumed (Kääb et al., 2021). Glacier thinning, rising equilibrium line altitudes and warming of the frozen bedrock bond in steep faces are documented and accelerating (Gruber and Haeberli, 2007; Hugonnet et al., 2021; Maurer et al., 2019).

Most hazard research addresses where the next failure will occur and how far the resulting flow will travel. A third question determines whether people live: once a cascade has started, how much of its travel time becomes usable warning? Sättele et al. (2015) formalised early-warning reliability as a chain in which detection, transmission and response each consume time, and Cook et al. (2021) demonstrated the detection half of that chain for Chamoli, showing that regional seismic networks resolved the flow at ranges up to 100 km and could in principle have supported downstream warning. What remains scarce is measurement of the realised chain, end to end, against a fatal event, because the necessary combination is seldom available. It requires an instrumentally constrained trigger time together with a documented downstream arrival chronology.

The 26 August 2026 Bhote Koshi–Trishuli disaster supplies that combination, on a massif with a recent and fatal mass-movement record: the 2015 Gorkha earthquake triggered an avalanche into Langtang village that killed more than 200 people, its runout amplified by anomalous winter snow (Fujita et al., 2017). The trigger has a reviewed seismic origin time, and Nepal's Flood Forecasting Division published a minute-resolution chronology of gauge failures, bulletin issuance and downstream arrivals. The flow travelled about 200 km of channel through a population whose exposure was broadly comparable along the corridor, while the available lead time varied by two orders of magnitude, so the corridor behaves as a natural experiment on lead time. The analysis is possible only because Nepal's Department of Hydrology and Meteorology (DHM) released a detailed technical situation report within a day of the event, while the emergency response was still under way. That report closes by recommending a technical review of the forecasting and early warning system, and specifically an analysis of the difference between the observed stage record and the preliminary forecasts. This paper is offered as a contribution to that review.

What follows is an assessment of an architecture rather than of the people who operated it. The limits identified here follow from where the instruments sit and how the decision path is wired, and they would constrain any downstream-gauge network in a catchment of this steepness. Staff acted on the information their instruments provided, and the notification that began the alert sequence came from a district office and from station staff whose own gauge was destroyed twenty minutes later. This paper measures the warning chain and does not simulate the flow, which is not yet supportable, as Sect. 5 sets out. The analysis rests only on open, citable observations.

2 Event and data

At 08:37:10 Nepal Time (NPT, UTC+05:45) on 26 August 2026 a combined ice and bedrock mass detached from the glaciated northern flank of the Langtang massif. The USGS reviewed catalogue (U.S. Geological Survey, 2026) lists the resulting signal as event `us7000tbwb`, M 5.2, at zero depth and event type `landslide`, and a second, smaller failure at the same location followed at 11:45:35 NPT as `us7000tc90`, M 4.2, also typed `landslide`. The GFZ reviewed solution (GFZ Helmholtz Centre for Geosciences, 2026) independently gives M_w 5.7 at the same origin and also types the event a landslide. Both are fixed-depth solutions on different magnitude scales, so neither constrains the mechanism beyond the event type each assigns, and the agreement on that type is what carries weight. Nepal's chronology logs the trigger instead as an M 4.4 earthquake attributed to the Department of Mines and Geology, which was the solution available domestically at the time. For roughly the first half hour, responders were therefore working from a tectonic interpretation, not from a mass movement with an inevitable downstream flood consequence. Distinguishing the two in real time is not routinely possible anywhere, and the reclassification followed later.

Four independent estimates of the initiation point agree within 3.5 km, and every one places the detachment inside Rasuwa district, 3.3 to 6.6 km south of the Nepal–China boundary (Table 1, Fig. 1). The flow path, by contrast, is transboundary, because the Lhende Khola drains north across the border, joins the Bhote Koshi in Gyirong County, Tibet Autonomous Region, China, and the combined flow re-enters Nepal at the Rasuwagadhi crossing. The source lies within Nepal's own jurisdiction. The blockage and the lake it impounded do not. Everything else about the source is contested, and Table 1 carries the reported values without resolving them. Volume is the one that matters here, and the figure in circulation describes the total mass mobilised along the runout, most of it channel and valley fill containing no glacier ice, so it sets no ice budget. Section 3.4 instead adopts a detachment volume bracketing the largest documented Himalayan bedrock–ice failures, and reports how the conclusion behaves if the detached mass were far larger. Expert assessments issued in the days after the event state that no pre-existing glacial lake drained, so the cascade was not a glacial lake outburst flood (ICIMOD, 2026; USGS, 2026).

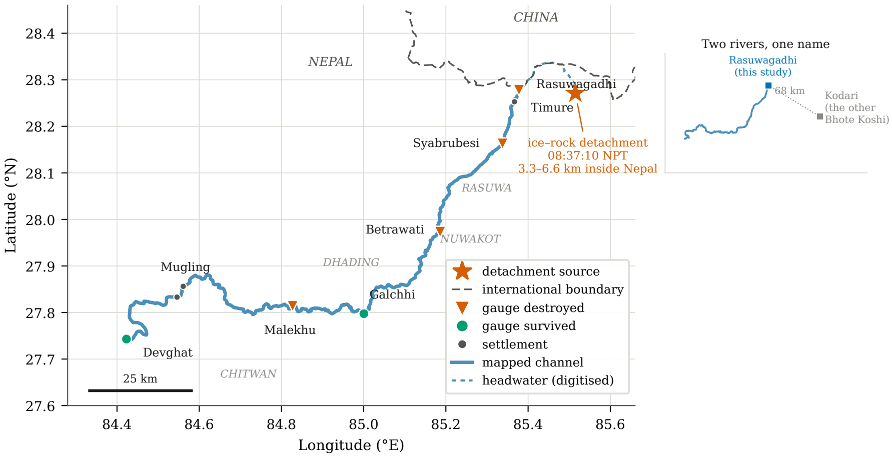

Figure 1. Study area, from OpenStreetMap channel and boundary data. The star marks the detachment source, 3.3 to 6.6 km inside Nepal, and the dashed segment the headwater reach, digitised independently at 22.3 km against the 20.1 to 24.0 km traced on terrain. Triangles are gauging stations destroyed on 26 August, circles those that survived. The inset distinguishes the two Nepali rivers named Bhote Koshi.

Table 1. Source and corridor parameters as reported, and the values used here. Reported source geometry disagrees between assessments made in the days after the event, and that disagreement is carried through, not averaged away.

Quantity	As reported	Used here
Initiation point	four estimates within 3.5 km	seismic solution
Position vs border	3.3 to 6.6 km south	inside Nepal
Detachment elevation	about 4880 m, or 5200 to 5400 m	4820 to 5070 m measured
Vertical drop	about 1200 m, or about 1830 m	carried as a range
Mobilised volume	more than 10^8 m^3, incl. entrainment	sets no ice budget
Detachment volume	not measured	10 to 30 $\times$ 10^6 m^3
Rasuwagadhi to Devghat	about 168 km (DHM)	178 km measured
Source to Rasuwagadhi	unmapped	20.1 to 24.0 km traced
Reach sinuosity	not reported	1.09 upper, 1.81 lower
Node to channel	–	within 0.6 km

The propagation record is the technical situation report issued by DHM's Flood Forecasting Division on the day, which gives a minute-resolution chronology, the official warning and danger thresholds at each station, and a discharge analysis at Devghat. The ten-minute stage series behind that report is still served by the department's river-watch pages, and it is retrieved here for every station on the corridor, so front arrival times here are read off the instruments themselves. Each station that survived brackets the front between its last sample at the local river level and the first sample risen above it, and each station destroyed brackets it between the last report it sent and the first it failed to send. The series reproduce the report's own telemetry-loss time at Betrawati, its peak of 6.57 m at Devghat and its danger crossing at Kali Khola, which is what licenses reading the rest of them. They also correct it. The national authority's situation report states that the Bhote Koshi station at Syabrubesi stopped transmitting at about 08:50 with a last level of 1.62 m (National Disaster Risk Reduction and Management Authority, 2026). That reading belongs to the station at Rasuwagadhi, whose warning stage is 6.0 m, while the Syabrubesi station last read 3.80 m against a 5.50 m warning stage. Two instruments have been reported as one in the official record, and the archive separates them.

Where the instrument record and the published chronology disagree, the instrument record is used. The chronology gives 15:20 at Devghat, where the station's own series sits at its local level until 14:30 and has risen by 14:40, so the published time falls mid-rise at 5.70 m rather than at the front. Every arrival time here, and every front velocity derived from one, therefore departs from the official chronology. That report was a rapid analysis issued within a day, while the response was running and on timings from stations being destroyed as it was written, and its purpose was to inform that response rather than to fix a chronology for later work. Readers comparing the two should expect the times to differ for that reason. Channel distances are measured along the OpenStreetMap river centreline by shortest path (OpenStreetMap contributors, 2026). Sinuosity varies enough between the upper gorge and the lower Narayani that a single corridor-wide value would misstate the lower reaches, so each reach is measured separately. Only the headwater segment above Rasuwagadhi is unmapped, so its length is traced on the Copernicus GLO-30 terrain model (European Space Agency, 2021), following steepest descent after depression filling from each of the four initiation estimates. The traces converge into one channel that loops north across the border, which is why the 13.5 km great-circle separation was never attainable, and calibration on the adjacent mapped reach, which the procedure overmeasures by about five percent, gives 20.1 to 24.0 km. The national authority independently describes the source as about 20 km upstream of Rasuwagadhi (National Disaster Risk Reduction and Management Authority, 2026), which falls at the lower edge of that range, and a centreline digitised independently from the scarp gives 22.3 km, close to its midpoint. The channel is braided and shifts within its valley floor between years, so no digitisation is definitive, and a flood follows the steepest grade rather than the low-flow centreline, which is why the length is traced and carried as a range that every dependent quantity inherits. Two names require care. Devighat hydropower station in Nuwakot, one of the damaged installations, is not Devghat in Chitwan and Tanahun, the downstream gauge used here. More consequentially for the literature, two Nepali rivers are named Bhote Koshi: the corridor studied here, which drains via Rasuwagadhi to the Trishuli and Narayani in the Gandaki basin, and a second river 68 km east draining via Kodari to the Sun Koshi. The historical outburst record discussed in Sect. 3.5 belongs to the second of these.

3 Results

3.1 The lead-time budget

In the chronology of Table 2, institutional latency, defined as the interval from the physical trigger to the mass public alert, was 38.8 min, while the wave reached the uppermost monitoring point within 12.8 min. That budget divides into three physically distinct segments. The first ended when the wave reached the gauge, and no domestic architecture could have detected the event before then by observing the river. A further 10.0 min passed between the first missing report, from the Rasuwagadhi gauge at 08:50, and notification of the Division at 09:00, which is the interval required to recognise a negative signal. The final 16.0 min, from notification to mass dispatch, is confirmation and administrative escalation. Faster procedures can shorten only the last two segments, because the first shrinks only if detection moves from the river to the source.

Lead time at Syabrubesi was -26 to -16 min. At Betrawati the last reading of 3.55 m at 09:20 sits inside that station's ordinary range for the week, so the front arrived after that reading, not before it, which places arrival between 09:20 and 09:30 and lead time between $+4$ and $+14$ min. Both settlements in the districts that recorded fatalities therefore had lead time at or below zero within observational uncertainty, while downstream of Betrawati it exceeded one hour everywhere. The alert itself was substantial in reach, but dispatch time is an upper bound on warning performance, because delivery, receipt and response times are not recorded. Under any response-time floor of the kind Sättele et al. (2015) treat as part of the chain, a lead time of a few minutes is not operationally useful, so the negative lead times reported here are conservative. The delay had two structural causes, the first being that the architecture is triggered by downstream gauges, so the first domestic indication was a missing report from Rasuwagadhi, a negative signal that must be distinguished from ordinary equipment failure before it can be acted on. The escalation path then ran from a district office through the national disaster authority to the meteorological department, with no machine-to-machine link at any step. No arrangement covered automatic notification across the border either, so no upstream signal could shorten the interval.

This gives the architecture a blind zone that no procedure can remove. A downstream-gauge architecture cannot warn any settlement upstream of its first gauge, and can warn those below it only by the margin between wave travel time and institutional latency. The flood front velocity over the reach from the source to Syabrubesi was 25 to 49 m s^{-1}, the width of that bracket set by the traced headwater and the ten-minute reporting cycle together, so the margin was negative along the entire inhabited upper corridor on any admissible reading. The front velocity then decays monotonically by a factor of three to ten, to 4.8 to 8.0 m s^{-1} between Kali Khola and Devghat (Fig. 2), which is the kinematic signature of a hyperconcentrated debris flow relaxing into a flood wave. Six stations enter that profile, each timing the front to within one reporting cycle, and the reaches between them carry no headwater uncertainty at all, because the unmeasured segment is a single offset shared by every node below it. The lowest reach is the widest for a different reason. Its downstream end is timed at the Devghat gauge, whose published position is given to two decimal places and cannot be placed on the channel, so the distance is measured to the confluence instead and the four kilometres between the two is carried as a position uncertainty. The upper-reach bracket meets the 16 to 25 m s^{-1} measured at comparable range at Chamoli (Shugar et al., 2021) at its lower end and reaches twice that at its upper, so this event was at least as fast and may have been much faster. An independent reconstruction recovers about 37 m s^{-1} in the headwater

Table 2. Chronology of the 26 August 2026 cascade. Times are NPT. Sources: USGS FDSN event web service for the seismic entries, and the DHM Flood Forecasting Division technical situation report for all others.

Time (NPT)	Δt	Event
08:37:10	0	Detachment, USGS `us7000tbwb`, M 5.2, type `landslide`
08:40	+2.8 min	Rasuwagadhi gauge, last transmission, 1.62 m
08:50	+12.8 min	Rasuwagadhi report missing. Syabrubesi gauge, last transmission, 3.80 m
09:00	+22.8 min	Syabrubesi report missing. District office and Betrawati station staff notify the Division
09:15	+37.8 min	Confirmation, first early warning issued
09:16	+38.8 min	Mass SMS dispatch, 679 295 messages to four districts
09:20	+42.8 min	Betrawati gauges, last transmission, 3.55 and 1.93 m
10:20	+102.8 min	Galchhi gauge begins to rise, peak 369.45 m at 10:50
11:26	+168.8 min	Phurke (Malekhu) gauge crosses its warning level
11:43	+185.8 min	Phurke station and adjacent bridge swept away
11:45:35	+188.4 min	Second detachment at the source, `us7000tc90`, M 4.2
13:10	+272.8 min	Kali Khola gauge begins to rise, danger level crossed 14:20
14:30	+352.8 min	Devghat gauge begins to rise
16:00	+442.8 min	Devghat peak, 6.57 m, 5850 $\mathrm{m^3\ s^{-1}}$

from trimline superelevation (geo-pera, 2026), a local flow velocity rather than a front velocity, obtained with no input from the chronology used here, and it falls inside the bracket the arrival times give.

Table 3 evaluates four alert architectures against the observed arrivals, and each assumed latency is stated as an assumption.

Table 3. Warning lead time in minutes by settlement under four alert architectures. Negative values indicate that the wave arrived before the alert. Architecture A is observed, while B, C and D are counterfactual with the assumed alert latencies stated in the text.

Architecture	Syabru.	Betra.	Galchhi	Malekhu	Mugling	Devghat
A observed	−26	+4	+72	+130	+224	+364
B border sensor	−2	+28	+96	+154	+248	+388
C seismic, 5 min	+8	+38	+106	+164	+258	+398
D seismic, 2 min	+11	+41	+109	+167	+261	+401

Architecture B assumes an in-channel sensor at the border reporting within 5 min of the wave reaching it. Architectures C and D assume source-side seismic detection with automated dissemination in 5 min and 2 min respectively. Operational debris-flow alarm systems reach detection-to-alarm intervals of about a minute in instrumented catchments (Badoux et al., 2009), and regional seismic networks have been shown to detect and locate flow events of this size within minutes (Cook et al., 2021). Both budgets sit inside those demonstrated capabilities. Landslides of this magnitude radiate long-period signals whose

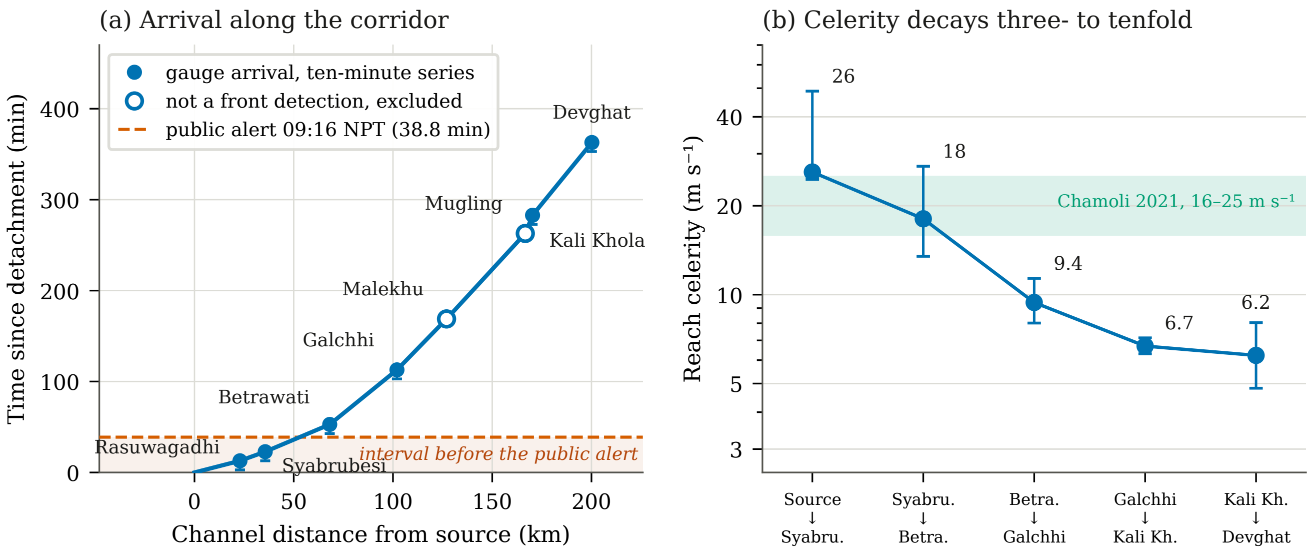

Figure 2. Propagation of the flood wave. (a) Arrival time against measured channel distance from the source. Filled markers are gauge arrivals read from the ten-minute stage series, open markers the two nodes timed by a threshold crossing and by a confirmed-past bound, neither of which detects the front, so both are excluded from the velocity estimates. Horizontal bars give the headwater distance range and vertical bars the arrival brackets set by station reporting cycles. The dashed line marks the mass public alert. (b) Flood front velocity, decaying by a factor of three to ten. Bars on the lowest reach include the position uncertainty of the Devghat gauge. The band shows Chamoli 2021 velocities at comparable range (Shugar et al., 2021).

force histories can be inverted from distant stations (Ekström and Stark, 2013), so the signal that a detector would act on is well characterised. Nepal's national network lies within about 100 km of the source, the range at which Cook et al. (2021) resolved the Chamoli event. Source-side detection is the only architecture tested that moves the first inhabited settlement across zero. Propagating the Syabrubesi arrival bracket, architecture C yields between +8 and +18 min there, and at Rasuwagadhi, which the wave reached between 2.8 and 12.8 min after the trigger, between −2 and +8 min, so the gain at the uppermost settlement is real but not assured. The gains further downstream of about 34 min at every settlement below Betrawati do not depend on either bracket. Architecture B needs restating against the instrument record, because the in-channel sensor it assumes is not hypothetical. A gauge stands at Rasuwagadhi, two kilometres inside the border, and it reported normally until the wave reached it. What the corridor lacked was not the sensor but a rule that reads its silence. For settlements within roughly ten minutes of travel time from a credible detachment source, the available instrument is siting.

3.2 The uppermost gauges were destroyed below their own thresholds

Latency accounts for only half of the failure. Table 4 sets the last recorded stage at each in-path station against that station's official warning and danger levels. None of the destroyed gauges registered the event. Rasuwagadhi was lost while reading

27 % of its warning stage, Syabrubesi 69 % and Betrawati 87 %, so a threshold-triggered system would have issued nothing from any of them. The fraction rises steadily downstream, which is what a wave outrunning its own detection network looks like on a threshold scale. The wave arrived faster than the sampling interval could resolve a rise, and the gauges passed from normal to destroyed without an intervening alarm state. Furthest downstream, Devghat peaked at 6.57 m against a 7.3 m warning threshold, so the station that survived, in the reach with hours of warning, also never crossed its trigger.

Table 4. Highest stage recorded at each in-path station against official DHM thresholds: for the stations lost, the last reading transmitted, and for those that survived, the event peak. Values are read from the department's ten-minute series. The Bhote Koshi has two stations, one at Rasuwagadhi and one at Syabrubesi, reported as one station in the official chronology and separated here from the department's own archive.

Station	Stage (m)	Warn (m)	Frac.	Outcome
Bhote Koshi at Rasuwagadhi	1.62	6.0	0.27	destroyed, never triggered
Bhote Koshi at Syabrubesi	3.80	5.5	0.69	destroyed, never triggered
Trishuli at Betrawati	3.55	4.1	0.87	destroyed, never triggered
Trishuli at Phurke (Malekhu)	10.48	7.0	1.50	triggered 11:26, swept 11:43
Trishuli at Kali Khola	12.35	10.8	1.14	triggered 14:20, survived
Narayani at Devghat	6.57	7.3	0.90	never triggered, survived

Destruction of monitoring infrastructure by the event it is meant to observe is itself a documented failure mode in this region, most directly at Melamchi in 2021, where the Nakote station recorded the flood and was then lost (Maharjan et al., 2021). What the present record adds is the quantified fraction of the station's own threshold at the moment of loss. A gauge destroyed after crossing its threshold has already discharged its warning function, whereas one destroyed at 27 % of threshold never entered the alarm logic at all. The monitoring requirement also does not end with the first failure, because a second detachment from the same source occurred at 11:45:35 NPT, minutes after the Phurke station and its adjacent bridge were swept away, so the source was still producing failures well inside the response window. In a corridor where the wave outruns the gauge network, stage thresholds are the wrong detection variable. The only quantity that rose fast enough to be diagnostic was the loss of telemetry itself. Treating that loss as a positive alarm condition, rather than an equipment fault to be investigated, is cheap and immediate. The objection is equally immediate. A destroyed station does not report that it has been destroyed, it simply stops reporting, which is what an ordinary radio or power failure also looks like, so a rule that fires on silence invites the false alarms that destroy confidence in a warning system. That objection can be measured instead of argued, because the service serves the days before the event as well.

Over the nine days of reporting that remain retrievable before the detachment, the six stations on the flow path dropped 34 reports in nine separate gap episodes, the longest 170 min at Syabrubesi and 100 min at Kali Khola. Episodes are the right unit, since a station offline for three hours is one alarm to an operator and not eighteen. A rule firing on a single missing report would therefore have raised about one alarm a day, which is unusable as a public trigger and is exactly the objection made good. A rule requiring two adjacent stations on the same reach to fall silent within thirty minutes raised none at all in the same nine days. Zero observed is not a rate of zero, and the one-sided 95 % Poisson limit for that count is 0.33 a day, so what the record supports is a separation of at least threefold between the two rules, not an absolute rate for the stricter one. The more useful question is how long a corroborated rule runs before it cries wolf. Treating each station's outages as an independent process of rate λ and duration d, two of them coincide within a window W at a rate of about $\lambda_1\lambda_2(d_1 + d_2 + 2W)$, which on the observed rates gives one false coincidence about every 144 days. Putting every rate at its upper limit at once shortens that to about seven days. Nine days of history cannot separate a wait of four months from a wait of five days, and that, rather than the count of zero, is the real limit on what this measurement establishes.

That separation is what makes the choice tractable, because the stricter rule was available on the day. The two Bhote Koshi stations fell silent at 08:50 and 09:00 as measured by the reports they failed to send, so a single-station rule was available at 08:50 and a two-station rule at 09:00. The first is twenty-six minutes before the public alert and ten before the Division was notified by telephone. The second is sixteen minutes before the alert and arrives at the same moment as the telephone call, so coincidence detection cost ten minutes here and bought an order of magnitude in specificity. Two caveats bound the result. It counts gaps as the archive now shows them, so a report that arrived late and was backfilled would look complete here while a detector watching in real time saw silence, which makes every rate above a lower bound. And the false-alarm advantage of coincidence assumes the failures are independent, which stations sharing power or backhaul are not under the conditions that produce the hazard. Both push the same way, toward the stricter rule and against reading these rates as transferable. The method transfers even where the numbers do not: any operator can run this measurement on their own reporting history before choosing a rule.

Neither rule makes six stations an adequate network for this hazard, and the measurement above is better read as a bound on what the existing instruments can support than as a design. Fluvial forecasting works in hours and has room for a sparse network with a human in the loop. A corridor whose first inhabited settlement lies thirteen minutes from a credible detachment source has neither. Two changes follow from the independence problem rather than from the arithmetic. Redundant instruments at a single point, on separate power and telemetry, would make the assumption behind coincidence detection defensible instead of merely untested, and would also let equipment failure be told apart from site destruction, which is the discrimination every rule considered here lacks. Instruments that fail informatively would help more than additional stations that fail silently, and a camera that stops returning frames while its co-located gauge still reports says something that neither says alone.

Neither idea is new to this country. The warning system installed below Tsho Rolpa in 1998 against the same hazard class used fully redundant sensing, so that several sensors had to fail before a false alarm or a missed event could occur, across seventeen warning stations in two valleys (Bell et al., 1999). It had ceased operating by 2002, which a later national assessment attributes in part to the lake having been lowered and the hazard being taken to have passed (International Centre for Integrated Mountain Development, 2011). Sensor count is also not by itself the binding constraint. A system installed in 2001 on the other river named Bhote Koshi, the one entering Nepal at Kodari, was assessed as yielding six minutes of warning because every station lay below the border, and the remedy identified was instruments in the upper catchment, which lies in the Tibet Autonomous Region, China, rather than more of them downstream (International Centre for Integrated Mountain Development, 2011). That is the same structural limit the present corridor shows, recorded a decade earlier on a neighbouring catchment, and it is why the blind zone is treated here as a property of where the instruments sit relative to the source rather than of how many there are.

3.3 Mortality follows lead time, body recovery does not

Reported fatalities concentrated in Rasuwa and Nuwakot, the reach where lead time was negative or negligible. Copernicus EMS grading of post-event imagery (Copernicus Emergency Management Service, 2026) records 323 buildings destroyed at Syabrubesi and 372 at Timure, both above the confluence, 2479 at Bidur and 397 at Phosretar on the Trishuli, with 3571 destroyed and 4685 graded as affected across the four areas mapped so far, two more having been requested and not yet delivered. A community of about 250 households in Rasuwa was reported destroyed in its entirety. The service classifies the imaged deposit as a mass movement, not as a flood, in every product delivered. Downstream, where lead time exceeded an hour, the wave still arrived with destructive force, reaching 12.3 m at Kali Khola and destroying the Phurke bridge, yet those districts contributed few deaths. The spatial basis of this claim requires care. No dataset of deaths by district of occurrence exists for this event, and the available district-resolved figure is bodies recovered, which is a recovery location and not a mortality location. Infrastructure supplies the check that mortality cannot, because a bridge cannot be carried downstream and counted somewhere else. Of 59 bridges surveyed along the corridor (Humanitarian OpenStreetMap Team, 2026), 23 of the 27 in Rasuwa were washed out, against 11 of 20 in Nuwakot, 5 of 8 in Dhading and none of the 3 in Gorkha. That inventory is still being compiled and does not separate the two middle districts reliably, but the contrast between the impact reach and the furthest downstream district is large and runs opposite to body recovery, which is what the two measures should do if impact was upstream and retrieval downstream. Mortality location is therefore inferred from where people were swept away, using that gradient, building-destruction counts, the destroyed resettlement community and agency statements, none of which is a mortality census. The inference is reported at that strength.

Recovery displaced downstream by 100 to 250 km. Totals were still rising through the compilation of this study, from 538 dead and 977 missing reported by NDRRMA at 15:00 NPT on 28 August to 1357 and 5326 by 8 September, the missing count falling at times as people were traced and rising as more were reported. Of bodies recovered, 359 were in Chitwan and 219 in Nawalparasi East against 140 in Rasuwa (Fig. 3b), with 121 taken from the Narayani alone. The displacement is real but it is not a fixed property of the event, and the nine revisions of this breakdown demonstrate why. The ratio between the district that received most bodies and the district where the wave began ran to about twenty by the third day, then fell to twelve, and now stands at under three as recovery reached the upper corridor. A snapshot of recoveries measures where retrieval had got to on the day it was taken. That is the reason the spatial inference above rests on the bridge gradient, which cannot be carried downstream, and not on this distribution. Only aggregate counts are used here, and no named missing-person registries were ingested. The missing are now resolved by district, and that measure runs the other way from recovery. Of 5326 people missing on 8 September, 2860 were registered in Rasuwa and 1981 in Nuwakot, the two districts where lead time was negative or negligible, with about 587 foreign nationals not attributed to a district. The figures given sum to 5428 against the stated total, an excess of 102 that is carried here rather than reconciled. Registration district is not proof of location when the wave arrived, so this is not a mortality census either, but it is a district-resolved measure of where people were lost rather than of where they were retrieved, and it points the same way as the bridge gradient. District mortuary capacity was exceeded roughly five- to eightfold in the districts that received the bodies. Hospital morgues in Chitwan hold 30 to 50 and an emergency facility for about 250 was required, which the district's 359 recoveries have since passed as well, while Kaski's combined capacity of 88 received 93 bodies transported from four other districts. The displacement of recovery from impact appears not to have been documented at this scale in the cascading-hazard literature, and it carries a direct operational consequence. For long-runout mountain cascades, mortuary and disaster-victim-identification capacity requires planning at basin scale, not at district scale, and search effort requires allocation to reaches that an impact model would not identify as affected.

What happened after the wave passed is a separate question from what this paper measures, and the two should not be read as one verdict. The national authority records 11 814 people rescued by 1 September, among them 253 foreign nationals, with 21 011 personnel deployed, and 14 461 people in two rural municipalities of Rasuwa cut off for up to six days by damage to roads, power and communications (National Disaster Risk Reduction and Management Authority, 2026). By 8 September the rescued figure stood at 13 583 and 6827 injured had been treated. That effort ran for weeks across five districts. What this paper measures is the thirty-nine minutes before the alert and the travel time available at each settlement below it, which is a question about where instruments sit and how a decision path is wired. It is settled before any responder can act.

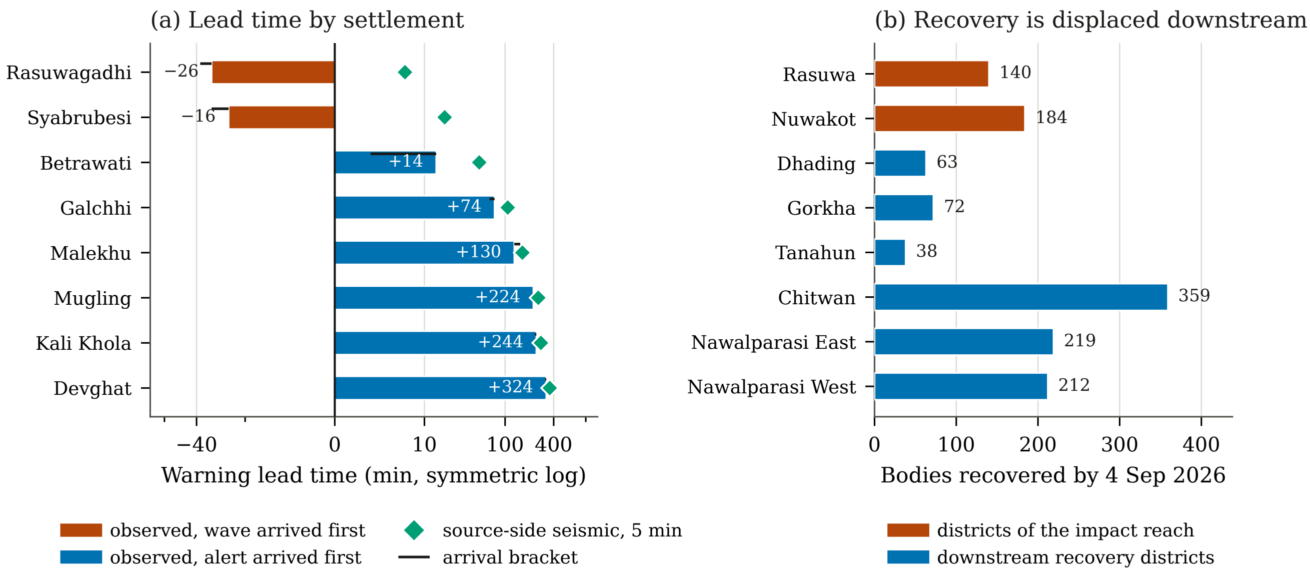

Figure 3. Lead time and its consequences. (a) Warning lead time at each settlement under the observed architecture, shown as bars, and under source-side seismic detection with a five-minute budget to public message, shown as diamonds, on a symmetric-log axis. Horizontal lines are arrival brackets. (b) Bodies recovered by district, ordered downstream. Five districts are as of midday on 3 September 2026 and three, Gorkha, Dhading and Tanahun, are carried from 1 September because that day's bulletin did not itemise them.

3.4 The frictional melt budget

Early commentary on this event raised the possibility that the energy of the fall melted the detached ice and that the meltwater became the flood. The proposition is testable in closed form, and two partitions of the frictional heat bracket the physics. Under a mass-proportional partition, each kilogram of the falling mass converts its own potential energy to heat where that heat is generated, so ice melts only from dissipation within the ice fraction, and the melt fraction f of the ice mass is

$$f = \frac{gH}{L_\mathrm{f} + c_\mathrm{i}\,\Delta T}, \qquad (1)$$

where g is gravitational acceleration, H the vertical drop, $L_\mathrm{f} = 3.34 \times 10^5$ J kg^{-1} the latent heat of fusion, $c_\mathrm{i} = 2100$ J kg^{-1} K^{-1} the specific heat capacity of ice and ΔT its initial temperature below freezing. Tabulating Eq. (1) for $H = 1200$ to 1830 m and ice initially between 0 and -10 °C gives $f = 3.3$ to 5.4 %. The sensitivity grid below spans the narrower 0 to -5 °C, which is the range the source elevation supports. Under an all-to-ice partition, every joule of the total mass's potential energy reaches the ice, with none lost to rock heating, comminution, air drag, acoustic radiation or the substrate, and the melt is capped by the ice actually present. The second is a strict thermodynamic ceiling rather than a physical expectation, and Chamoli shows that it can be approached, because frictional heating there melted nearly all of the ice in an 80:20 rock-to-ice mass (Shugar et al., 2021), which under this formulation requires roughly 70 % of the total potential energy to have reached the ice over the full runout drop. The flood volume is measured independently at Devghat. DHM computed a peak discharge of 5850 m^3 s^{-1} at 16:00 against an antecedent discharge of 2600 m^3 s^{-1}, giving 57.40×10^6 m^3 of total flow past the station. Removing the antecedent discharge leaves 19.96×10^6 m^3, which is the volume the event itself delivered and the quantity the melt comparison below uses. These are rating-curve quantities derived from stage during a sediment-laden flood with four upstream stations destroyed, and hyperconcentrated flow and event-scale channel change can shift such a rating by tens of per cent. The department confirms on enquiry that the most recent rating it holds for this station dates from 2023, three years before the event, and that it holds none at all for Galchhi, which is why that station contributes an arrival time here and no discharge. The conclusion below is insensitive to that uncertainty, as the margins show.

For detachments of 10 to 30×10^6 m^3 at ice fractions of 0.2 to 0.5, frictional melt yields 0.06 to 0.74×10^6 m^3 under the mass-proportional partition, which is 0.3 to 3.7 % of the flood, and 0.62 to 3.78×10^6 m^3 at the thermodynamic ceiling, which is 3.1 to 18.9 % (Fig. 4a). The inverse statement is stronger because it needs no assumption about the heat partition at all. Supplying 19.96×10^6 m^3 of water requires melting 21.8×10^6 m^3 of ice completely, and the entire Chamoli 2021 detachment contained about 5.4×10^6 m^3 of ice, being 27×10^6 m^3 at 20 % ice by volume, so the requirement is four times that, with every gram melted and none surviving into the deposit. Complete melting would match the flood only at bulk detachment volumes of 44 to 109×10^6 m^3 for ice fractions of 0.5 to 0.2. Imposing the energy constraint raises the requirement further, to 0.4 to 0.6 km^3 of ice under the mass-proportional partition.

The bound is conditional on the detached volume, and the condition is worth stating plainly. If the detached ice-bearing mass were as large as 10^8 m^3, the ceiling would rise to 31 to 63 % of the flood and frictional melt could not be excluded on these grounds. That figure is the total mobilised mass including entrained channel and valley fill, which contains no glacier ice,

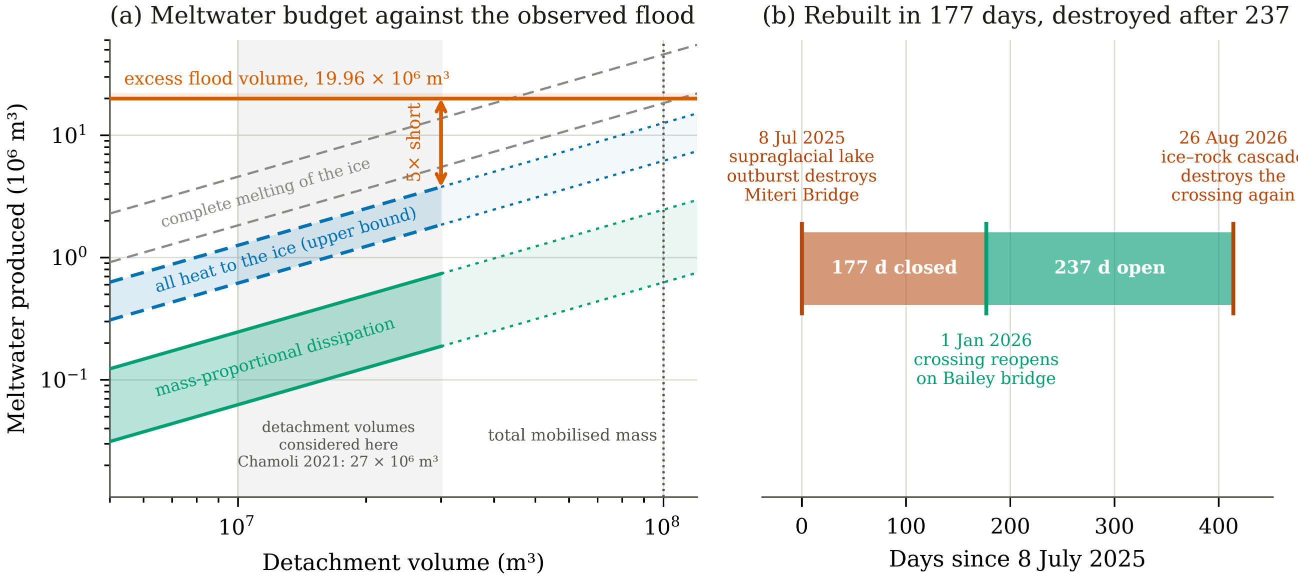

Figure 4. Water source and reconstruction cycle. (a) Meltwater produced by frictional dissipation against detachment volume. The green band is the mass-proportional partition and the blue band the upper bound in which all frictional heat reaches the ice, each spanning ice fractions of 0.2 to 0.5, drops of 1200 to 1830 m and initial ice temperatures of 0 to $-5\,^{\circ}$C. Both fade beyond 3×10^7 m^3, where the axis ceases to describe an ice-bearing detachment. Grey dashed lines show complete melting with no energy constraint, and the arrow marks the shortfall at the most favourable corner of the parameter space, where the upper bound still falls five-fold short of the observed flood volume shown in orange. (b) The Rasuwagadhi crossing between the two events, destroyed on 8 July 2025, reopened after 177 days and destroyed again after 237 days in operation.

and a detachment of 10^8 m^3 at 30 % ice would imply 30×10^6 m^3 of glacier ice leaving a single face, larger than the whole Chamoli detachment. Resolving this requires differencing the source-area topography, which the open imagery record does not currently permit. That measurement is the decisive test of the melt hypothesis and is stated here as a falsifiable prediction.

Within the adopted volume range, at least 80 % of the flood water, and more plausibly over 95 %, was not frictional meltwater. It was pre-existing channel water at monsoon stage, pore water in entrained saturated sediment, and water impounded behind the blockage and released on its failure. Available data do not constrain the partition among these three, though a transit to Syabrubesi of at most 22.8 min limits the impoundment-and-breach interval to the order of minutes, which argues that the impounded share was modest. The event is an avalanche-induced channel blockage and breach, in the lineage of Sedongpu (Li et al., 2022) and the rockfall-triggered outburst at Barun (Byers et al., 2019). For reference, the potential energy of 10 to 30×10^6 m^3 falling 1200 to 1830 m at a bulk density of 2000 kg m^{-3} is 2.4×10^{14} to 1.1×10^{15} J, equivalent to M 6.4 to 6.8 if fully radiated seismically, against an observed M 5.2. Only a small fraction of that energy reaches the seismic wavefield, so magnitude alone underestimates mass, which is part of why the trigger was first logged as a moderate earthquake. Once a detachment is detected, the quantity that governs downstream consequence is the blockage and its impoundment. A minutes-scale breach favours a transient, permeable blockage that overtopped and incised rapidly over a sustained landslide dam, and that is a falsifiable statement. An independent hydraulic reconstruction has since routed the alternative and found that a sustained dam and breach reaches the border half an hour to an hour late and peaks near a third of the measured trimline heights, while a blockage failing within minutes and a direct debris flow both remain admissible (geo-pera, 2026). The residual blockage subsequently impounded a barrier lake in Gyirong County, China, that reached about 2×10^6 m^3 and an overtopping state within 24 h, prompting a Level-IV alert and suspension of rescue operations on both sides of the border. It drained on 30 August.

3.5 Reconstruction cycle against hazard recurrence

This corridor was destroyed 414 days earlier. On 8 July 2025 an outburst from a previously uncatalogued supraglacial lake at about 5150 m on the Chinese side of the border, some 36 km upstream of Rasuwagadhi, destroyed the Miteri Sino-Nepal Friendship Bridge and the Rasuwagadhi dry port and damaged seven hydropower projects. The lake had grown from a small pond in December 2023 or 2024 to 0.64 to 0.75 km^2 by June 2025, according to the joint DHM and ICIMOD assessment. The border closed for 177 days at a reported cost exceeding NPR 22 bn in lost import revenue, and reopened on 1 January 2026 on a 91 m Bailey bridge built with Chinese support, then operated for 237 days (Fig. 4b). The 2026 event damaged 14 hydropower projects totalling about 748 MW and destroyed 40 to 42 km of the only overland road connecting Kathmandu to the Chinese border at Rasuwagadhi, which is the kind of concentrated exposure that Schwanghart et al. (2016) quantified for Himalayan hydropower against outburst floods. Damage figures are provisional press reports from the days immediately after the event. The same 40 km of valley was therefore struck twice by physically independent cryospheric mechanisms, first supraglacial lake drainage and then bedrock–ice detachment with channel blockage and breach.

The regional context requires the disambiguation noted in Sect. 2. The frequently cited outburst record of 1935, 1964 and 1981, and the 2016 Gongbatongshacuo event that Cook et al. (2018) showed to be measurable as a driver of fluvial erosion, all belong to the Poiqu basin, which drains to the other Bhote Koshi and thence to the Sun Koshi at Kodari, about 68 km east of Rasuwagadhi and in a different river system. No documented outburst record exists for the Trishuli corridor before 2025, and absence of record is not absence of events, because this corridor was ungauged and lightly reported before the dry port was built. The two histories together support the regional argument that both transboundary Bhote Koshi corridors are outburst-prone, and they do not support a single-channel recurrence series.

Exposure in this corridor is partly a product of the previous disaster. The community described in Sect. 3.3 had been resettled on the low-lying banks of the Trishuli after the 2015 Gorkha earthquake, so post-disaster reconstruction placed those households on the active floodplain of a river whose upstream hazard was already documented. Return-period design is poorly suited to this setting, because it treats each mechanism separately and assumes stationarity, so it does not represent the joint cryospheric hazard at a point. The operational arithmetic is simpler, in that rebuilding took 177 of the 414 days between the two events, or 43 % of the interval, and the replacement crossing operated for 237 days before the second event destroyed it. An independent study of the same two events reaches both intervals exactly, from its own sources and for the customs yard rather than the crossing (Li et al., 2026). Its parallel chain for the road bridge gives 173 and 241 days, which is a useful caution:

the crossing is one thing in ordinary speech and several assets operationally, and the interval depends on which is counted. The reconstruction was carried out quickly and under acute pressure to restore a trade route on which the district depends, and the design question it leaves is how to carry an interval this short into the next rebuild, alongside cost and lead time.

4 Discussion

The results converge on one design conclusion, and the downstream hydrology sharpens it. DHM assessed the Devghat stage as corresponding to a 2 to 3 year return period, a stage-based agency assessment adopted here as such and not independently verified. By the time the wave had travelled 200 km it was, in conventional flood-frequency terms, an ordinary event, and it never crossed the Devghat warning threshold. The lethal zone was defined by the reach in which no warning could physically arrive, so magnitude does not explain the mortality pattern while lead time does. That inference has a limit worth stating. Along a single flow path, lead time and flow intensity are collinear, because the near field had both the shortest warning and a hyperconcentrated debris flow at 25 to 49 m s^{-1}, while the far field had hours of warning and an ordinary flood wave. Near-field mortality may therefore have been intensity-limited as well as warning-limited. Exposure is a third confounder, since an independent terrain-envelope analysis places about 15 850 residents within 80 m of the channel in Nuwakot against 1317 in Rasuwa (Keystone GIS, 2026), so absolute counts by district reflect who was beside the river as well as when the message arrived. This design cannot separate the two. The failure occurred at 08:37 in daylight, which is favourable for evacuation and makes the absence of warning, and not the impossibility of response, the operative constraint, and exposure was concentrated by the resettlement described in Sect. 3.5 in precisely the reach with no lead time. Neither consideration resolves the collinearity, which a per-reach exposure normalisation would address once population and building data at that scale are available.

Nepal's current architecture rests on downstream gauges and on a manual escalation path. The event destroyed three of those gauges within the first 43 minutes and two never crossed a threshold. Three changes follow, in priority order. The most important is automated source-side seismic triggering, meaning continuous discrimination of surface-source signals in the glacierised headwaters, wired to public dissemination without a human relay. It is the only architecture tested here that places the first inhabited settlement on the positive side of zero, it exploits a detection capability already demonstrated at this range by Cook et al. (2021), and because the source lies inside Nepal it requires no cross-border agreement. The second change is to treat telemetry loss as an alarm condition in its own right, as Sect. 3.2 sets out. It costs nothing to implement, and on this network the corroborated form of the rule, two adjacent stations silent together, would have advanced domestic detection by sixteen minutes against the public alert while raising no false alarm in the nine days measured. The third change is machine-to-machine notification for the blockage and the barrier lake, which formed on the Chinese side of the border and are the specific hazard that such notification would address. Where no achievable warning latency helps, as at Timure and Rasuwagadhi, the available instruments are land-use restriction, elevated alignment for critical crossings, and a decision not to rebuild the same assets on the same terraces.

Pre-failure deformation monitoring would not have solved the timing problem. At Chamoli, optical feature tracking resolved 20 to 30 m of horizontal pre-collapse displacement over roughly the five years before failure, concentrated in summer, and the same study states that the timing of collapse could not have been forecast from satellite data alone (van Wyk de Vries et al., 2022). Systematic screening of Himalayan slopes on this basis is nonetheless feasible and overdue (Ahmed et al., 2026). Susceptibility and timing are different problems, because interferometry and feature tracking can identify which slopes above which settlements deserve instrumentation and land-use attention, and could not have identified 26 August as the day. That is why the post-failure lead-time budget is the operative quantity.

A further observation concerns the evidence base itself. Three days after the event, Nepal's machine-readable disaster database carried eight flood incidents for the affected corridor whose linked loss records totalled zero deaths and zero missing, and no event record had yet been opened for the cascade. Every casualty figure in circulation, including those used here, therefore traces to situation reports and press releases, not to the structured portal. This is a predictable consequence of load, because the same staff who would populate the database were conducting the response, and the portal depends on the same manual reporting path as the warning chain. Both are limited by that path, which is an argument for automating the entry of agency-issued figures rather than a criticism of the agencies compiling them. The record here documents the state of the portal on 29 August 2026, and it may since have been backfilled.

The same corridor produced two floods in 414 days from mechanisms that current inventories treat as unrelated. Glacial lake inventories (Veh et al., 2020; Shugar et al., 2020; Taylor et al., 2023) would not have flagged an ice–rock detachment, and detachment inventories (Kääb et al., 2021) would not have flagged a supraglacial pond that formed within eighteen months. Corridors such as this one require joint cryospheric hazard assessment at reach scale, integrating lake growth, slope stability and blockage potential. Haeberli et al. (2017) made the same argument for de-glaciating ranges where degrading permafrost creates new lakes and destabilises the slopes above them, and the multihazard framing after Melamchi 2021 called for it as well (Maharjan et al., 2021; Kargel et al., 2016). The boundary condition is the state of the catchment itself. Langtang has lost 41.5 % of its glacier area since the Little Ice Age, its rate of loss has more than quadrupled, and warming there is elevation-dependent, running at about 0.3 °C decade^{-1} above 4000 m against 0.1 °C decade^{-1} lower down (Silwal et al., 2026). That gradient concentrates change on exactly the elevations where these failures begin, and the same deglaciation is projected to raise outburst risk across the Third Pole (Zheng et al., 2021).

5 Limitations

Several analyses that would strengthen this work are not yet supportable, so they are excluded here. No hydrodynamic simulation is offered, because there is no calibrated digital elevation model, no measured inflow hydrograph and no field validation, so any depth or velocity field would be uncalibrated. Reconstructing the cascade properly would need the sequence of source-volume, two-phase runout and hydrodynamic models that Lala et al. (2018) applied to an outburst process chain elsewhere in the Nepal Himalaya, with a solver able to carry the solid and fluid phases together (Mergili et al., 2017). The inputs that sequence needs do not yet exist for this event. No detachment volume is estimated either, and the open imagery record explains why. Two independent releases cover the event, sixteen and twenty-six very-high-resolution scenes by 1 September and both still growing (Vantor, 2026; Planet Labs PBC, 2026), reaching 0.55 m and including an acquisition three hours after the failure, so neither resolution nor latency is the deficiency. One stereo pair was released, two WorldView-3 strips of 27 August carrying camera models, held outside the scene index. Its footprint reaches Syabrubesi but stops about 0.6 km west of the source, so it constrains the corridor surface and not the scar. The source is imaged twice after the event, at 3.4 and 3.8 m under 81 to 88 % cloud, and never before it, so this record carries no before-and-after pair there. Medium-resolution imagery does, and a rapid third-party analysis differences Sentinel-2 across the failure to report about 100 ha of ice loss beside the seismic hypocentre (A. Soto, 2026). That is a planform area, and neither Sentinel mission carries elevation information. What the volume needs is a pair of surfaces, and half of that pair now exists: a Pleiades tri-stereo model of the source area at 2 m, acquired in October 2019 and released openly days after the event (Berthier, 2026). It covers all four initiation estimates, and its elevations corroborate the lower of the two reported detachment heights while reaching nothing near the upper one. A post-event surface has not been released, so the detached volume remains unmeasured, and the constraint is now a single missing acquisition rather than an absence of data. The most recent open pre-event scene containing Syabrubesi predates the failure by three months.

The timing data carry more uncertainty than their reported precision suggests. Gauge nodes are bracketed only within their ten-minute reporting cycle, the Mugling entry is logged as confirmed-past and is therefore an upper bound on front arrival, and Malekhu is timed by a threshold crossing, which follows the front by an unknown margin. The last two are excluded from the velocity profile for that reason. Where a station was destroyed, the front is bracketed by the report it failed to send, which assumes the front is what disabled it rather than a power or backhaul failure minutes ahead of the water. These are propagated into the velocity ranges and the lead-time brackets, and they are the reason the counterfactual gain at Syabrubesi is reported as a range and not as a single value. The mortality-location claim rests on inference, as Sect. 3.3 sets out, and the collinearity of lead time with flow intensity along a single corridor is not resolved by this design. No formal attribution is offered either, and the documented warming and destabilisation context is reported without asserting a fraction of attributable risk. No antecedent-meteorology claim is made either, because circulating accounts of a preceding warm spell are not yet supported by gauge or reanalysis evidence. Casualty figures remain provisional, and the analysis uses only their spatial distribution, which is stable across revisions, together with aggregate counts.

6 Conclusions

The mass public alert followed the physical trigger by 38.8 minutes while the wave reached the uppermost gauge within 12.8 minutes, giving a lead time of -26 to -16 min at Syabrubesi and between $+4$ and $+14$ min at Betrawati. Reported fatalities concentrated in those two districts, while districts warned hours in advance received most of the bodies. Three destroyed gauges were lost at 27, 69 and 87 % of their warning stages, so threshold logic never fired, and the only signal that did travel at the speed of the event, the loss of telemetry, enters the system as an equipment fault rather than as a hazard signal. The two uppermost stations fell silent ten minutes apart, so even a rule demanding corroboration from a second station was available sixteen minutes before the alert went out, and over the nine days before the event that rule raised no false alarm while a rule firing on one missing report would have raised about one a day. Automated source-side seismic detection with a five-minute budget to public message would have delivered between $+8$ and $+18$ min at Syabrubesi instead of -26 to -16, and about 34 additional minutes at every settlement below Betrawati. Because the detachment occurred inside Nepal, that measure requires no cross-border agreement.

Frictional melting of the detached ice cannot account for the flood. Supplying the 19.96×10^6 m^3 excess volume measured at Devghat would require complete melting of 21.8×10^6 m^3 of ice, four times the ice content of the entire Chamoli 2021 detachment. The water came from the channel and from impoundment behind a transient blockage, which relocates the post-detachment monitoring target from the glacier to the blockage. At Devghat the event corresponded to a 2 to 3 year return period on DHM's assessment and never crossed the station's warning threshold. Rebuilding the Rasuwagadhi crossing consumed 177 of the 414 days between two destructive events from independent cryospheric mechanisms, and the replacement operated for 237 days before it was destroyed. An interval this short belongs in the design case for the replacement asset, alongside its cost and lead time.

Every measurement here was made from records the operating agencies already publish, an instrument archive and a chronology issued while the response was still under way. The same assessment can therefore be made on other networks before an event rather than after one.

Code availability. The analysis that produces every figure and table in this paper is archived at 10.5281/zenodo.22679444, release 3.0.0, under CC-BY-4.0. That is the exact version the results here were computed from. The concept DOI 10.5281/zenodo.22153581 always resolves to the newest release. The code is written in Python and relies on NumPy (Harris et al., 2020) and Matplotlib (Hunter, 2007).

Data availability. The data package underlying every figure, table and number in this paper is archived at 10.5281/zenodo.22679444, release 3.0.0, under CC-BY-4.0, with the concept DOI 10.5281/zenodo.22153581 resolving to the newest release. Each field in it carries its own source and evidence grade, so any value here can be traced to the record it came from. Five sources supply everything. Seismic origin times, locations, magnitudes and event classification come from the USGS Advanced National Seismic System Comprehensive Catalog (U.S. Geological Survey, 2026), and the event overview and runout distance from the USGS Landslide Hazards Program (USGS, 2026). The chronology, the official gauge thresholds, the discharge analysis and the flood volume come from the technical situation report issued on 26 August 2026 by the Flood Forecasting Division of Nepal's Department of Hydrology and Meteorology. No permanent public URL was located for it, so it was obtained through contemporaneous reproductions whose quoted figures agree with one another, and the copy used is archived with the data. The channel centreline, the international boundary and all settlement coordinates come from OpenStreetMap (OpenStreetMap contributors, 2026). Building damage comes from the grading products of Copernicus Emergency Management Service activation EMSR927 (Copernicus Emergency Management Service, 2026), and casualty and recovery figures from NDRRMA and Nepal Police situation reports of 28 and 29 August 2026. Personal data of disaster victims were deliberately excluded. Named missing-person registries and hospital and rescue manifests that were publicly reachable during the response were not ingested, and only aggregate counts appear anywhere in the archive.

Author contributions. Contributions are described using the CRediT taxonomy. SA was responsible for conceptualisation, data curation, formal analysis, investigation, methodology, software, validation, visualisation and writing of the original draft. AP contributed investigation, validation and review and editing: he reproduced the analysis independently, digitised the channel centreline used to check the traced headwater, verified the front arrival times and station stages read from the gauge archive, and identified the terminology and internal inconsistencies corrected in revision. Both authors reviewed and approved the submitted manuscript. No funding was acquired, and no supervision or project administration by others applies to this work.

Competing interests. The authors declare that they have no competing interests.

Acknowledgements. The Department of Hydrology and Meteorology and NDRRMA of Nepal released operational chronologies during an active emergency, ICIMOD provided rapid technical assessment, and the USGS Landslide Hazards and Earthquake Hazards Programs and the Copernicus Emergency Management Service released data openly and immediately. The maintainers of OpenStreetMap are gratefully acknowledged. This paper records the loss of the four hydrological stations destroyed in this event, and of the personnel and communities of the Bhote Koshi–Trishuli corridor.

Financial support. This research received no external funding.

References

A. Soto: Bhote Koshi avalanche source detection from Sentinel-1 and Sentinel-2, Rapid analysis, code and output published on GitHub, https://github.com/asoto59g/Nepal, last access: 30 August 2026, 2026.

Ahmed, R., Bhardwaj, A., Sam, L., and Van Tricht, L.: Ice-rock avalanches in a warming Himalaya indicate pathways toward effective preparedness, Communications Earth & Environment, 7, 217, https://doi.org/10.1038/s43247-026-03352-y, 2026.

Badoux, A., Graf, C., Rhyner, J., Kuntner, R., and McArdell, B. W.: A debris-flow alarm system for the Alpine Illgraben catchment: design and performance, Natural Hazards, 49, 517–539, https://doi.org/10.1007/s11069-008-9303-x, 2009.

Bell, W. W., Donich, T., Groves, K. L., and Sytsma, D.: Tsho Rolpa GLOF warning system project, in: Proceedings of the 28th IAHR World Congress, Graz, https://www.iahr.org/library/infor?pid=13718, last access: 6 September 2026, 1999.

Berthier, E.: 13 October 2019 Pléiades (CNES) pre-event digital elevation models for the rock-ice avalanche source area of the August 2026 Trishuli catastrophic flood, Dataset, Zenodo. Images from the Pléiades World Heritage programme of Dinamis and CNES; processed with the Ames Stereo Pipeline, https://doi.org/10.5281/zenodo.22147118, cC-BY-4.0, last access: 1 September 2026, 2026.

Byers, A. C., Rounce, D. R., Shugar, D. H., Lala, J. M., Byers, E. A., and Regmi, D.: A rockfall-induced glacial lake outburst flood, Upper Barun Valley, Nepal, Landslides, 16, 533–549, https://doi.org/10.1007/s10346-018-1079-9, 2019.

Cook, K. L., Andermann, C., Gimbert, F., Adhikari, B. R., and Hovius, N.: Glacial lake outburst floods as drivers of fluvial erosion in the Himalaya, Science, 362, 53–57, https://doi.org/10.1126/science.aat4981, 2018.

Cook, K. L., Rekapalli, R., Dietze, M., Pilz, M., Cesca, S., Rao, N. P., Srinagesh, D., Paul, H., Metz, M., Mandal, P., Suresh, G., Cotton, F., Tiwari, V. M., and Hovius, N.: Detection and potential early warning of catastrophic flow events with regional seismic networks, Science, 374, 87–92, https://doi.org/10.1126/science.abj1227, 2021.

Copernicus Emergency Management Service: EMSR927: Flood in Nepal, grading products for Syapru Besi, Timure and Bidur, European Commission, Joint Research Centre, Copernicus EMS Rapid Mapping, https://mapping.emergency.copernicus.eu/activations/EMSR927/, last access: 29 August 2026, 2026.

Ekström, G. and Stark, C. P.: Simple scaling of catastrophic landslide dynamics, Science, 339, 1416–1419, https://doi.org/10.1126/science.1232887, 2013.

European Space Agency: Copernicus Global Digital Elevation Model GLO-30, Produced using WorldDEM data of Airbus Defence and Space; free and open under the Copernicus data policy, https://doi.org/10.5270/ESA-c5d3d65, last access: 1 September 2026, 2021.

Fujita, K., Inoue, H., Izumi, T., Yamaguchi, S., Sadakane, A., Sunako, S., Nishimura, K., Immerzeel, W. W., Shea, J. M., Kayastha, R. B., Sawagaki, T., Breashears, D. F., Yagi, H., and Sakai, A.: Anomalous winter-snow-amplified earthquake-induced disaster of the 2015 Langtang avalanche in Nepal, Natural Hazards and Earth System Sciences, 17, 749–764, https://doi.org/10.5194/nhess-17-749-2017, 2017.

geo-pera: Reconstruction of the 26 August 2026 Bhote Koshi outburst flood from open satellite data, Rapid reconstruction, code under MIT licence, https://github.com/geo-pera/bhotekoshi-2026-reconstruction, last access: 29 August 2026, 2026.

GFZ Helmholtz Centre for Geosciences: GEOFON event `gfz2026qrfy`: Nepal–China border region (landslide), GEOFON Program, GFZ Helmholtz Centre for Geosciences, Potsdam, https://geofon.gfz.de/eqinfo/event.php?id=gfz2026qrfy, last access: 29 August 2026, 2026.

Gruber, S. and Haeberli, W.: Permafrost in steep bedrock slopes and its temperature-related destabilization following climate change, Journal of Geophysical Research: Earth Surface, 112, F02S18, https://doi.org/10.1029/2006JF000547, 2007.

Haeberli, W., Schaub, Y., and Huggel, C.: Increasing risks related to landslides from degrading permafrost into new lakes in de-glaciating mountain ranges, Geomorphology, 293, 405–417, https://doi.org/10.1016/j.geomorph.2016.02.009, 2017.

Harris, C. R., Millman, K. J., van der Walt, S. J., Gommers, R., Virtanen, P., Cournapeau, D., Wieser, E., Taylor, J., Berg, S., Smith, N. J., Kern, R., Picus, M., Hoyer, S., van Kerkwijk, M. H., Brett, M., Haldane, A., del Río, J. F., Wiebe, M., Peterson, P., Gérard-Marchant, P., Sheppard, K., Reddy, T., Weckesser, W., Abbasi, H., Gohlke, C., and Oliphant, T. E.: Array programming with NumPy, Nature, 585, 357–362, https://doi.org/10.1038/s41586-020-2649-2, 2020.

Hugonnet, R., McNabb, R., Berthier, E., Menounos, B., Nuth, C., Girod, L., Farinotti, D., Huss, M., Dussaillant, I., Brun, F., and Kääb, A.: Accelerated global glacier mass loss in the early twenty-first century, Nature, 592, 726–731, https://doi.org/10.1038/s41586-021-03436-z, 2021.

Humanitarian OpenStreetMap Team: Nepal flood 2026: flood affected area, Bhote Koshi and Trishuli, Humanitarian Data Exchange, Open Database License (ODbL), https://data.humdata.org/dataset/hot_flood_npl, last access: 29 August 2026, 2026.

Hunter, J. D.: Matplotlib: a 2D graphics environment, Computing in Science & Engineering, 9, 90–95, https://doi.org/10.1109/MCSE.2007.55, 2007.

ICIMOD: Major flash flood sweeps through Nepal's Rasuwa district, raising fears of further downstream flooding, Press release, International Centre for Integrated Mountain Development, Kathmandu, https://www.icimod.org/press-release/major-flash-flood-sweeps-through-nepals-rasuwa-district-raising-fears-of-further-downstream-flooding/, last access: 28 August 2026, 2026.

Immerzeel, W. W., Lutz, A. F., Andrade, M., Bahl, A., Biemans, H., Bolch, T., Hyde, S., Brumby, S., Davies, B. J., Elmore, A. C., Emmer, A., Feng, M., Fernández, A., Haritashya, U., Kargel, J. S., Koppes, M., Kraaijenbrink, P. D. A., Kulkarni, A. V., Mayewski, P. A., Nepal, S., Pacheco, P., Painter, T. H., Pellicciotti, F., Rajaram, H., Rupper, S., Sinisalo, A., Shrestha, A. B., Viviroli, D., Wada, Y., Xiao, C., Yao, T., and Baillie, J. E. M.: Importance and vulnerability of the world's water towers, Nature, 577, 364–369, https://doi.org/10.1038/s41586-019-1822-y, 2020.

International Centre for Integrated Mountain Development: Glacial lakes and glacial lake outburst floods in Nepal, Tech. rep., ICIMOD, Kathmandu, world Bank document 98829. https://documents1.worldbank.org/curated/en/150061467986261271/pdf/98829-WP-Box393178B-PUBLIC-Glacial-lakes-and-glacial-late-outburst-floods-in-Nepal.pdf, last access: 6 September 2026, 2011.

Kääb, A., Leinss, S., Gilbert, A., Bühler, Y., Gascoin, S., Evans, S. G., Bartelt, P., Berthier, E., Brun, F., Chao, W.-A., Farinotti, D., Gimbert, F., Guo, W., Huggel, C., Kargel, J. S., Leonard, G. J., Tian, L., Treichler, D., and Yao, T.: Massive collapse of two glaciers in western Tibet in 2016 after surge-like instability, Nature Geoscience, 11, 114–120, https://doi.org/10.1038/s41561-017-0039-7, 2018.

Kääb, A., Jacquemart, M., Gilbert, A., Leinss, S., Girod, L., Huggel, C., Falaschi, D., Ugalde, F., Petrakov, D., Chernomorets, S., Dokukin, M., Paul, F., Gascoin, S., Berthier, E., and Kargel, J. S.: Sudden large-volume detachments of low-angle mountain glaciers, more frequent than thought?, The Cryosphere, 15, 1751–1785, https://doi.org/10.5194/tc-15-1751-2021, 2021.

Kargel, J. S., Leonard, G. J., Shugar, D. H., Haritashya, U. K., Bevington, A., Fielding, E. J., Fujita, K., Geertsema, M., Miles, E. S., Steiner, J., Anderson, E., Bajracharya, S., Bawden, G. W., Breashears, D. F., Byers, A., Collins, B., Dhital, M. R., Donnellan, A., Evans, T. L., Geai, M. L., Glasscoe, M. T., Green, D., Gurung, D. R., Heijenk, R., Hilborn, A., Hudnut, K., Huyck, C., Immerzeel, W. W., Liming, J., Jibson, R., Kääb, A., Khanal, N. R., Kirschbaum, D., Kraaijenbrink, P. D. A., Lamsal, D., Shiyin, L., Mingyang, L., McKinney, D., Nahirnick, N. K., Zhuotong, N., Ojha, S., Olsenholler, J., Painter, T. H., Pleasants, M., Pratima, K. C., Yuan, Q. I., Raup, B. H., Regmi, D., Rounce, D. R., Sakai, A., Donghui, S., Shea, J. M., Shrestha, A. B., Shukla, A., Stumm, D., van der Kooij, M., Voss, K., Xin, W., Weihs, B., Wolfe, D., Lizong, W., Xiaojun, Y., Yoder, M. R., and Young, N.: Geomorphic and geologic controls of geohazards induced by Nepal's 2015 Gorkha earthquake, Science, 351, aac8353, https://doi.org/10.1126/science.aac8353, 2016.

Keystone GIS: Bhote Koshi flash flood impact and exposure atlas, Nepal, 26 August 2026, Version 7, Zenodo, https://doi.org/10.5281/zenodo.22118798, last access: 29 August 2026, 2026.

Lala, J. M., Rounce, D. R., and McKinney, D. C.: Modeling the glacial lake outburst flood process chain in the Nepal Himalaya: reassessing Imja Tsho's hazard, Hydrology and Earth System Sciences, 22, 3721–3737, https://doi.org/10.5194/hess-22-3721-2018, 2018.

Li, M.-L., Yin, H., Liu, Y., Zheng, Y., Yu, Z., and Hu, F.: Data and reproducibility materials for "Beyond source-specific GLOF hazard maps: a two-event empirical stress test of infrastructure exposure in the Gyirong–Trishuli trans-Himalayan corridor", Dataset, Zenodo, https://doi.org/10.5281/zenodo.22269502, cC-BY-4.0, last access: 3 September 2026, 2026.

Li, W., Zhao, B., Xu, Q., Scaringi, G., Lu, H., and Huang, R.: More frequent glacier-rock avalanches in Sedongpu gully are blocking the Yarlung Zangbo River in eastern Tibet, Landslides, 19, 589–601, https://doi.org/10.1007/s10346-021-01798-z, 2022.

Maharjan, S. B., Steiner, J. F., Shrestha, A. B., Maharjan, A., Nepal, S., Shrestha, M. S., Bajracharya, B., Rasul, G., Shrestha, M., Jackson, M., and Gurung, S.: The Melamchi flood disaster: cascading hazard and the need for multihazard risk management, Tech. rep., ICIMOD, Kathmandu, https://doi.org/10.53055/icimod.981, 2021.

Maurer, J. M., Schaefer, J. M., Rupper, S., and Corley, A.: Acceleration of ice loss across the Himalayas over the past 40 years, Science Advances, 5, eaav7266, https://doi.org/10.1126/sciadv.aav7266, 2019.

Mergili, M., Fischer, J.-T., Krenn, J., and Pudasaini, S. P.: r.avaflow v1, an advanced open-source computational framework for the propagation and interaction of two-phase mass flows, Geoscientific Model Development, 10, 553–569, https://doi.org/10.5194/gmd-10-553-2017, 2017.

National Disaster Risk Reduction and Management Authority: Rasuwa-Bhotekoshi flood: search, rescue and relief response, situation report #01, Ministry of Home Affairs, Government of Nepal, 1 September 2026, 09:00. https://ndrrma.gov.np/mediafiles/rasuwa/Rasuwa_Flood_SitRep_Temp_ENG_01_01092026.pdf, last access: 6 September 2026, 2026.

OpenStreetMap contributors: Planet dump retrieved from https://planet.openstreetmap.org, Open Database License (ODbL); river centreline, international boundary and settlement data retrieved through the Overpass API, https://www.openstreetmap.org, last access: 28 August 2026, 2026.

Planet Labs PBC: Planet crisis response: Bhote Koshi–Trishuli outburst flood, Nepal, 2026, Source Cooperative, Creative Commons Attribution-NonCommercial 4.0, https://source.coop/planet/disasterdata/nepal-flash-flood-2026-08-26, last access: 29 August 2026, 2026.

Sättele, M., Bründl, M., and Straub, D.: Reliability and effectiveness of early warning systems for natural hazards: concept and application to debris flow warning, Reliability Engineering & System Safety, 142, 192–202, https://doi.org/10.1016/j.ress.2015.05.003, 2015.

Schwanghart, W., Worni, R., Huggel, C., Stoffel, M., and Korup, O.: Uncertainty in the Himalayan energy–water nexus: estimating regional exposure to glacial lake outburst floods, Environmental Research Letters, 11, 074 005, https://doi.org/10.1088/1748-9326/11/7/074005, 2016.

Shugar, D. H., Burr, A., Haritashya, U. K., Kargel, J. S., Watson, C. S., Kennedy, M. C., Bevington, A. R., Betts, R. A., Harrison, S., and Strattman, K.: Rapid worldwide growth of glacial lakes since 1990, Nature Climate Change, 10, 939–945, https://doi.org/10.1038/s41558-020-0855-4, 2020.

Shugar, D. H., Jacquemart, M., Shean, D., Bhushan, S., Upadhyay, K., Sattar, A., Schwanghart, W., McBride, S., van Wyk de Vries, M., Mergili, M., Emmer, A., Deschamps-Berger, C., McDonnell, M., Bhambri, R., Allen, S., Berthier, E., Carrivick, J. L., Clague, J. J., Dokukin, M., Dunning, S. A., Frey, H., Gascoin, S., Haritashya, U. K., Huggel, C., Kääb, A., Kargel, J. S., Kavanaugh, J. L., Lacroix, P., Petley, D., Rupper, S., Azam, M. F., Cook, S. J., Dimri, A. P., Eriksson, M., Farinotti, D., Fiddes, J., Gnyawali, K. R., Harrison, S., Jha, M., Koppes, M., Kumar, A., Leinss, S., Majeed, U., Mal, S., Muhuri, A., Noetzli, J., Paul, F., Rashid, I., Sain, K., Steiner, J., Ugalde, F., Watson, C. S., and Westoby, M. J.: A massive rock and ice avalanche caused the 2021 disaster at Chamoli, Indian Himalaya, Science, 373, 300–306, https://doi.org/10.1126/science.abh4455, 2021.

Silwal, G., Davies, B., Carr, J. R., King, O., Buzzard, S., Carrivick, J. L., and Baral, P.: Glacier changes in Langtang Catchment, Central Nepalese Himalaya from the Little Ice Age (~1815 CE) to 2023 CE, Global and Planetary Change, 264, 105 555, https://doi.org/10.1016/j.gloplacha.2026.105555, 2026.

Taylor, C., Robinson, T. R., Dunning, S., Carr, J. R., and Westoby, M.: Glacial lake outburst floods threaten millions globally, Nature Communications, 14, 487, https://doi.org/10.1038/s41467-023-36033-x, 2023.

U.S. Geological Survey: Advanced National Seismic System (ANSS) Comprehensive Catalog of earthquake events and products, U.S. Geological Survey Earthquake Hazards Program [data set], events `us7000tbwb` and `us7000tc90`, retrieved through the FDSN event web service, https://doi.org/10.5066/F7MS3QZH, https://earthquake.usgs.gov/earthquakes/search/, last access: 28 August 2026, 2026.

USGS: 2026 Nepal debris avalanche and flash flood, Landslide Hazards Program, U.S. Geological Survey, https://www.usgs.gov/programs/landslide-hazards/science/2026-nepal-debris-avalanche-and-flash-flood, last access: 28 August 2026, 2026.

van Wyk de Vries, M., Bhushan, S., Jacquemart, M., Deschamps-Berger, C., Berthier, E., Gascoin, S., Shean, D. E., Shugar, D. H., and Kääb, A.: Pre-collapse motion of the February 2021 Chamoli rock–ice avalanche, Indian Himalaya, Natural Hazards and Earth System Sciences, 22, 3309–3327, https://doi.org/10.5194/nhess-22-3309-2022, 2022.

Vantor: Open data: Nepal flooding, August 2026, Vantor (formerly Maxar) Open Data Program, Creative Commons Attribution-NonCommercial 4.0, https://vantor-opendata.s3.amazonaws.com/events/Nepal-Flooding-Aug-2026/collection.json, last access: 29 August 2026, 2026.

Veh, G., Korup, O., and Walz, A.: Hazard from Himalayan glacier lake outburst floods, Proceedings of the National Academy of Sciences of the United States of America, 117, 907–912, https://doi.org/10.1073/pnas.1914898117, 2020.

Zheng, G., Allen, S. K., Bao, A., Ballesteros-Cánovas, J. A., Huss, M., Zhang, G., Li, J., Yuan, Y., Jiang, L., Yu, T., Chen, W., and Stoffel, M.: Increasing risk of glacial lake outburst floods from future Third Pole deglaciation, Nature Climate Change, 11, 411–417, https://doi.org/10.1038/s41558-021-01028-3, 2021.